Recent Trends of Fluorescence Lifetime Imaging Microscopy Analysis Using Machine Learning

Ilya D. Shchechkin[1,2]
[1] Privolzhsky Research Medical University, Institute of Experimental Oncology and Biomedical Technologies, 10/1 Minin and Pozharsky sq., Nizhny Novgorod 603950, Russian Federation
[2] N.I. Lobachevsky Nizhny Novgorod National Research State University, 23 Gagarina ave., Nizhny Novgorod 603022, Russian Federation
e-mail: Iliahasa1992@gmail.com

Abstract. Fluorescence Lifetime Imaging Microscopy (FLIM) is an advanced imaging technique that provides quantitative information about molecular interactions and changes in the microenvironment by measuring the emission decay lifetimes of molecules undergoing fluorescence. The integration of FLIM with machine learning holds great promise for advancing biomedical research and clinical diagnostics by enabling precise quantification of cellular processes and microenvironmental changes. As FLIM instrumentation becomes more accessible and analytical methods continue to improve, the technique is poised to have a significant impact across various fields of biology and medicine. This review considers a range of methods of applying Machine Learning to FLIM data processing.

Keywords: deep learning; segmentation; denoising; upscaling.

Paper #9185 received 24 Oct 2024; revised manuscript received 21 Jan 2025; accepted for publication 19 Feb 2025; published online 23 Mar 2025. doi: 10.18287/JBPE25.11.010201.

1 Introduction

Fluorescence Lifetime Imaging Microscopy (FLIM) is a cutting-edge imaging technique that leverages the unique fluorescence lifetime of molecules to provide valuable insights into biological processes at the molecular level. When combined with Machine Learning (ML), FLIM imaging opens up new frontiers in biomedical research and diagnostics by enabling the precise analysis and interpretation of this type of complex fluorescence data.

FLIM is an advanced imaging technique that utilizes the fluorescence lifetime of molecules to generate images based on differences in the decay rates of their excited states. Unlike traditional imaging methods that rely on emission spectra, FLIM creates contrast based on the lifetimes of individual fluorophores. The fluorescence lifetime represents the average time a molecule remains in an excited state before returning to the ground state by emitting a photon [1].

FLIM works by capturing a 2D grid of pixels in the sample, where the fluorescence lifetime of each pixel is determined using time-correlated single photon counting (TCSPC). This involves aiming an excitation laser at each spot, collecting emission photon arrival times, and sorting them into a histogram to extract the fluorescence lifetimes mathematically. By including fluorescence lifetime information, FLIM not only enhances image contrast but also provides additional insights into the local environment, molecular interactions, and various cellular processes that are not accessible through intensity imaging alone [1]. The principle of obtaining FLIM data is presented in Fig. 1.

The advantage of FLIM over intensity-based methods lies in its robustness against factors like concentration, sample absorption, and excitation intensity, making it a powerful tool for functional imaging across different biological contexts. By using picosecond timescales for excitation and detection, FLIM achieves high temporal resolution, enabling the study of processes that occur on the scale of a few nanoseconds. Furthermore, fluorescence lifetime is sensitive to the local environment of the fluorophore, including factors such as pH, temperature, viscosity, and the presence of quenching molecules [2].

By mapping the fluorescence lifetimes across a sample, FLIM can reveal important information about the distribution and interactions of biomolecules within cells and tissues. For example, FLIM has been used to study protein-protein interactions via Förster resonance energy transfer (FRET), to monitor changes in cellular metabolism, and to image oxygen concentrations [3].

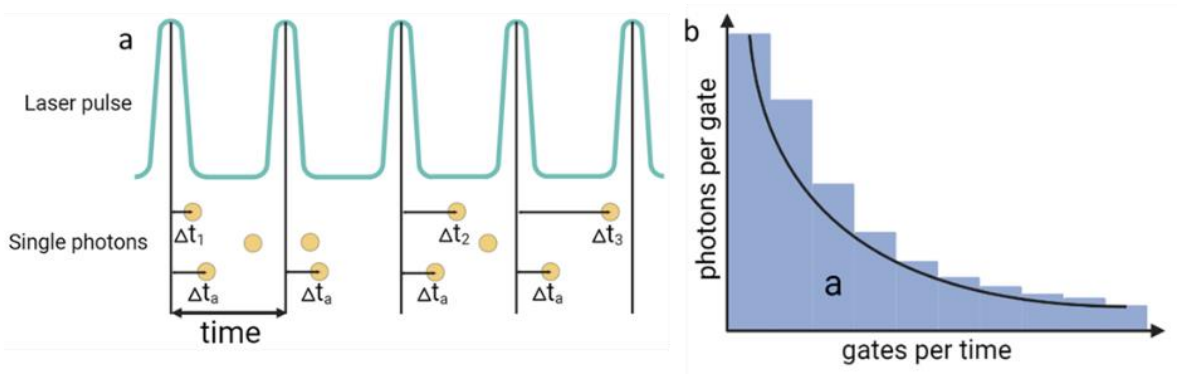

Fig. 1 The principle of obtaining FLIM microscopy data: (a) the principle of operation of TCSPC; (b) approximation of the fluorescence decay curve.

FLIM visualization has further advantages. FLIM provides quantitative data on molecular interactions and changes in the microenvironment by enabling the detection of minor changes in the lifetimes of fluorescence, and allowing simultaneous visualization of several fluorophores with different lifetimes. FLIM can even be used for label-free imaging based on endogenous fluorophores.

Multiphoton microscopy and FLIM are powerful techniques for investigating cellular metabolic dynamics in both *in vivo* and *ex vivo* settings. FLIM is particularly notable for its non-invasive nature, high sensitivity, and the ability to visualize cellular physico-chemical parameters—such as viscosity, temperature, and pH − without the need for exogenous stains [1, 4].

As an example, FLIM has been particularly useful for evaluating metabolic activity by analyzing the fluorescence lifetimes of endogenous fluorophores such as nicotinamide adenine dinucleotide (NAD(P)H). This molecule exists in two forms: NADH, which is the reduced form, and NAD+, its oxidized counterpart. These forms play crucial roles in metabolic pathways, including glycolysis, the tricarboxylic acid cycle, and oxidative phosphorylation. Specifically, NADH is linked to ATP production in the cytosol through glycolysis, and in mitochondria via oxidative phosphorylation. Additionally, its phosphorylated form, NADPH, is integral to biosynthetic pathways involving lipids, amino acids, and nucleotides, as well as to the glutathione cycle, which protects against reactive oxygen species [5].

Recent advancements in FLIM have enhanced the assessment of metabolic permutations, allowing for a more nuanced understanding of cellular metabolism. For instance, one study demonstrated that expanding the traditional two-lifetime model of NADH to a four-lifetime model evaluating the four components of fluorescence decay and, accordingly, a larger number of studied molecules significantly improved metabolic assessment. This approach allowed the researchers to quantitatively map changes in mitochondrial and cytosolic NADH concentrations and binding states, providing insights into the metabolic state of individual cells in response to pharmacological stimuli, such as during the browning of white adipose tissue [6].

Furthermore, FLIM can evaluate multiple metabolic parameters simultaneously, such as to provide the fluorescence-lifetime redox ratio (FLIRR), which reflects the relative concentrations of NADH and flavin adenine dinucleotide (FAD) in cells. This capability enables the detection of distinct metabolic states and variations within cellular compartments, thereby facilitating the investigation of metabolic dysfunctions in various biological contexts, including cancer and aging [7].

The integration of advanced computational tools for analyzing FLIM data also allows for the quantification of spatial heterogeneity in metabolic activity, revealing patterns that are critical for understanding complex biological processes [1, 8].

Additionally, FLIM has shown promise for clinical diagnostics, as changes in tissue fluorescence lifetimes can be indicative of pathological conditions such as cancer. A key concept that enhances the utility of FLIM in oncology is the Warburg effect. This phenomenon describes the tendency of cancer cells to preferentially rely on glycolysis for energy production, even when oxygen is available. This metabolic shift results in distinct changes in the cellular microenvironment, including variations in pH, ion concentrations, and the presence of specific metabolites. Consequently, these alterations affect the fluorescence characteristics of the tissue, including significant changes in fluorescence lifetimes [9]. FLIM has shown remarkable potential for early cancer detection, as it can differentiate between healthy and malignant tissues based on their fluorescence lifetimes. Research has also demonstrated its ability to identify cancerous lesions in various tissues, including oral and skin cancers, with high sensitivity and specificity [10]. The technique's ability to provide label-free, non-invasive imaging makes it an attractive option for *in vivo* applications [9].

However, FLIM visualization also has some limitations. The necessary data analysis requires specialized equipment and experience. FLIM may work more slowly than other image acquisition methods. Noise sensitivity can limit the accuracy of measurements over the equipment's entire service life.

While FLIM has traditionally been limited by the complexity of the instrumentation and the time-

consuming data analysis required, recent advances in detector technology and the development of deep-learning-based analysis methods have helped to address these challenges [11]. As a result, FLIM is becoming more accessible and practical for a wider range of biomedical applications.

Machine learning is a widely used approach for analyzing various types of biomedical images. When implementing the FLIM method, there are several techniques and neural network architectures available for image enhancement and analysis. This article will discuss methods of machine learning that can be used to improve and interpret the results of FLIM.

2 FLIM-Image Preprocessing

The raw data obtained from FLIM can be noisy and require significant preprocessing to enhance image quality and ensure accurate analysis. The primary objective of FLIM data preprocessing is to improve signal quality through denoising and other enhancement techniques.

2.1 Denoising FLIM Images

There are many techniques for the denoising of FLIM images using non-convolutional, convolutional filters, machine- and deep-learning methods.

Non-convolutional filters are techniques used in image processing that do not rely on the convolution operation to modify or enhance images. Instead, these filters often involve direct manipulation of pixel values based on specific algorithms or criteria. An example of non-convolutional filter is presented in Fig. 2.

(a) (b)

Fig. 2 NL-means denoising experiment with a natural image [12]: (a) noisy image with standard deviation 20, (b) restored image. Reprinted under the Creative Commons CC BY license from Ref. [12]).

Median filtering is a powerful technique for denoising FLIM images. The median filter operates by considering a local window around each pixel in the image, collecting the pixel values within that window, sorting them in ascending order, and replacing the center pixel value with the median value. This process is repeated for all pixels in the image. The median filter is particularly effective in removing small spatial disruptions to a signal while preserving the overall shape. It is also useful for removing outliers and anomalous jumps in values, making it a suitable choice for denoising FLIM data [13].

Non-local Means (NL-Means) filtering is a further effective image denoising algorithm that computes the filtered value of a pixel as a weighted average of all pixels in the image, determined by the similarity of small image patch centered at pixel of interest, effectively reducing Gaussian noise while preserving edges and details by adding “method noise”. That noise looks like white noise. The use of the rotationally invariant patch distance and guided image filtering for efficiency, make the technique particularly useful for denoising scientific images such as microscopy data in various applications unlike the use of local filters that take the mean value of a group of surrounding pixels [12, 13].

Moving Average Filter is a filter that replaces each pixel’s value with the average of its neighboring pixels. It is a simple way to smooth an image and reduce noise. Commonly used in time-series data smoothing and basic image noise reduction [14].

Bilateral Filter is a further filter smooths images while preserving edges by considering both the spatial distance and pixel intensity difference when averaging pixel values. It is often used in medical imaging to enhance structures without losing details, because it is effective at reducing noise while maintaining sharp edges [15].

Adaptive Filters is a specific filter that adjust their behavior based on the characteristics of the local image area. For example, adaptive median filters change their size based on the amount of noise detected. It is useful in scenarios where noise characteristics vary across an image due to its more effectiveness than static filters in non-uniform noise conditions [16, 17].

Convolutional filters, or kernels, are small matrices applied to an image to perform various operations such as blurring, sharpening, edge detection, denoising and more. The process involves sliding the filter over the image and computing a weighted sum of the pixels in the neighborhood defined by the filter. The result is a new image where each pixel value is derived from its surrounding pixels.

Convolutional filters can be categorized based on their function:

- Edge detection filters, such as Sobel and Prewitt filters, which highlight areas of rapid intensity change. The Sobel filter is one of the most widely used edge detection methods. It consists of two 3×3 kernels: one for detecting horizontal edges and another for vertical edges. The horizontal kernel emphasizes changes in intensity from left to right, while the vertical kernel focuses on changes from top to bottom. This method calculates the gradient magnitude and direction at each pixel, effectively highlighting edges. Similar to the Sobel filter, the Prewitt filter uses two 3×3 kernels for horizontal and vertical edge detection. It operates by convolving the input image with these kernels to approximate the gradient, helping to identify edges [18, 19].
- Blur filters, like Gaussian or Box filters that smooths images by averaging pixel values. The Box Blur

filter calculates the average of all pixels in a defined neighborhood (kernel) around each pixel. This filter treats all pixels equally and is simple to implement but can produce a loss of detail. Gaussian Blur uses a Gaussian function to assign weights to the pixels in the kernel, giving more importance to the central pixel and less to those further away [20].

- Sharpening filters, like the Laplacian, High Boost or Unsharp filters which enhances edges and fine details. The Laplacian filter is a second-order derivative operator that detects edges by calculating the second derivative of the image intensity. It highlights regions of rapid intensity change, making it effective for sharpening. High boost filtering enhances high-frequency components while preserving low-frequency information. Unsharp masking involves subtracting a blurred version of the image from the original image, which enhances edges. The process typically involves three steps: blurring the original image, subtracting this blurred image from the original, and then combining the results to enhance sharpness [21−23].

Convolutional filters are utilized in various applications, to improving visual quality through sharpening or blurring, to identifying edges and shapes for object detection and recognition, for separating different regions within an image for analysis.

Phasor analysis provides a graphical representation of FLIM data, where each pixel is represented as a point in the phasor plot, enabling the application of image processing techniques like median filtering to the phasor component images for effective denoising, while preserving spatial resolution. This helps in revealing hidden fluorescence components obscured by noise or background, and allowing for segmentation, based on clustering pixels with similar phasor coordinates, using unsupervised methods like *K*-means. It offers a "fit-free" approach that avoids complex curve-fitting procedures and provides quantitative information about the sample, with the linear properties of the phasor transformation enabling simple yet powerful denoising and analysis of the FLIM data [24].

Recent studies have demonstrated the application of Convolutional Neural Networks (CNNs) for denoising FLIM images. These networks are trained to enhance the signal-to-noise ratio (SNR) in FLIM data, which is crucial for accurate phasor measurements. By integrating CNNs with fast data acquisition systems, researchers have achieved significant improvements in image clarity and segmentation accuracy [25].

CNNs are utilized for denoising FLIM images after training on pairs of noisy and clean FLIM images to improve the signal-to-noise ratio and to handle the mixed Poisson-Gaussian noise common in FLIM data acquired using TCSPC. This CNN-based denoising approach, that includes transfer learning with pre-trained models like DnCNN, effectively enhances FLIM measurements, providing faster processing speeds and accurate, phasor-based segmentation for improved analysis, leveraging the benefits of transfer learning to avoid the need for extensive FLIM-specific training datasets, while still efficiently handling noise in the FLIM data [26, 27].

A transfer learning scheme that involves training a denoiser with synthetic noise data and then transferring this knowledge to denoise real-noise images, enhances the generalization ability of the denoising method. The approach leverages both adaptive instance normalization and transfer learning to improve denoising performance, allowing a denoiser trained with synthetic noise to effectively denoise real-noise images. This transfer learning scheme demonstrates robust performance even with a small number of labeled data, showcasing the effectiveness of transfer learning in FLIM denoising tasks. Such an approach leverages the powerful feature extraction capabilities of CNNs trained on large datasets like the Fluorescence Microscopy Dataset (FMD) [28].

These denoising techniques, combined with machine learning and deep learning approaches have shown promising results in enhancing the quality of FLIM images and enabling more accurate analysis of fluorescence lifetime data, which can be performed using transfer learning from pre-trained models on large datasets like the Fluorescence Microscopy Dataset (FMD).

2.2 Spatial Resolution Improvement

The conversion of low-resolution (LR) FLIM images to high-resolution (HR) images involves various techniques, including mathematical algorithms and NN-powered methods.

One approach to such resolution improvement is "single-sample image-fusion up-sampling" (SiSIFUS) that combines data from a low-resolution time-resolved detector and a high-resolution camera to achieve super-resolution in FLIM. Key points in this respect are the ability of FLIM to provide detailed information on molecular interactions but its limited resolution at high speeds due to time-resolved imaging constraints. The method merges data from a low-resolution time-resolved detector (measuring photon arrival times) and a high-resolution camera (measuring intensity) to computationally achieve super-resolution. It incorporates statistically informed priors to address the inverse retrieval problem, avoiding the hallucination risks, incorrect or misleading results that models generate, resulting from in traditional data-driven methods. The resulting enhanced images surpass those from standard bilinear interpolation, offering a versatile solution applicable to various image super-resolution challenges where there are two distinct datasets available [29]. An example of method implementation is presented in Fig. 3.

Another approach is sensor fusion implementation that combines data from a low spatial resolution but high temporal precision single-photon avalanche diode (SPAD) array with data from a CMOS camera that has high spatial resolution but no temporal resolution. This allows the reconstruction of time-resolved images at significantly higher spatial resolution than the SPAD input, upsampling by factors up to 12×12 in simulations and 4×4 experimentally. The method works by optically

blurring the image on the SPAD array to ensure temporal information from the entire field of view is captured, despite the low fill-factor of such SPAD arrays. Computational sensor fusion and optimization are then used to reconstruct a high resolution time-resolved image cube. The technique has been demonstrated for both LIDAR applications and FLIM studies of fluorescent cancer cells. It can fill in holes from dead SPAD pixels and remains robust against noise and ambient light. The main limitation is the long reconstruction time required post-measurement [30].

A further approach is a technique involving a two-channel attention network (TCAN) that leverages spatial representations and frequency contents to map low-resolution images to high-resolution ones effectively. This approach is designed to overcome limitations in current super-resolution fluorescence microscopy, such as the requirement for special fluorophores, complex optical systems, and lengthy acquisition and computational processes. The TCAN model is robust and can adapt to changes in pixel size and imaging setups, allowing it to generalize across different fluorescence microscopy modalities not included in the training data. The algorithm has been tested on various biological structures and dual-color confocal images, successfully improving resolution from around 230 nm to approximately 110 nm. This technique enables live-cell super-resolution imaging, and has provided detailed insights into the structures and dynamic behaviors of micro-tubules [31].

A separate method has been described that involves training neural networks to generate massive semi-synthetic FLIM data sets representing various cellular morphologies, sizeable dynamic lifetime ranges, and complex decay components. A degrading model is then used to obtain LR-HR pairs, and a hybrid neural network, the improved spatial resolution FLIM net (SRI-FLIMnet), is developed to simultaneously estimate both the fluorescence lifetimes and to realize the nonlinear transformation from LR to HR images. The evaluative results demonstrate SRI-FLIMnet's superior performance in reconstructing spatial information from limited pixel resolution. This approach has been verified using experimental images of bacterial-infected raw macrophage cells from mice, showing that the proposed data generation method and SRI-FLIMnet efficiently achieve superior spatial resolution for FLIM applications [32].

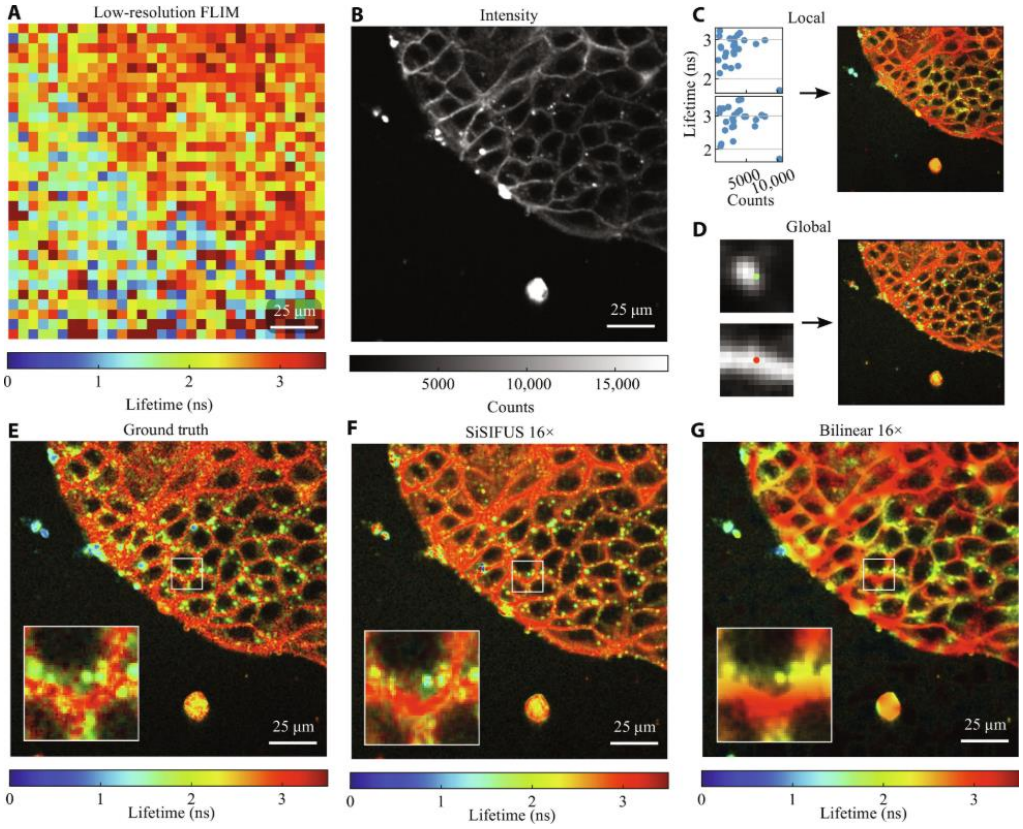

Fig. 3 Upsampling (16 × 16) of Madin-Darby canine kidney cells. (a) Low-resolution fluorescence lifetime image (32×32) of MDCK cells expressing Flipper-TR dye. (b) Corresponding high-resolution intensity image (512×512) of the sample. (c) Windows (5×5) of low-resolution FLIM are fitted to corresponding intensity values to generate an LP image (two example windows are shown). (d) A GP image is generated from 13×13 intensity patches with central FLIM measurements (two examples are shown). (e) The GT high-resolution FLIM target, intensity-weighted for visualization. (f) The proposed method, upsampling the low-resolution measurement by a factor of 16×16. (g) Bilinear interpolation upsampling the FLIM measurement by 16×16 [29]. Reprinted under the Creative Commons CC BY license from Ref. [29].

3 FLIM Analysis Using Machine Learning Techniques

FLIM image analysis includes obtaining fluorescence decay parameters for selected objects in the image in order to evaluate changes in the lifetimes, and accordingly the distribution of the fluorescent molecule being studied. The decay parameters are calculated for each pixel in the image, this being followed by the selection of a region of interest (ROI) for calculation of its own decay parameters as an average of the corresponding pixels.

The extraction of true lifetime values from the raw data takes place using traditional methods such as Maximum Likelihood Estimation and Least Squares fitting of fluorescence decay curves.

Maximum Likelihood Estimation (MLE) is a statistical method that estimates the parameters of a probability distribution by maximizing the likelihood function. For FLIM data, MLE is used to estimate the parameters of the fluorescence decay curve, such as the lifetime and amplitude. MLE is particularly useful when dealing with low photon counts, as it provides unbiased estimates of the decay parameters [33].

Least Squares (LS) fitting is a method that minimizes the sum of the squared differences between the observed data and the fitted model. In FLIM data analysis, LS fitting is therefore used to estimate the parameters of the fluorescence decay curve by minimizing the difference between the observed decay and the fitted exponential function. LS fitting is computationally efficient and widely used in FLIM data analysis software [34].

Both MLE and LS fitting are iterative methods that start with an initial estimate of the decay parameters and refine them until the best fit is obtained. The resulting fitted parameters are then used to generate the true lifetime images, where each pixel represents the estimated lifetime of the fluorophore.

These conventional curve-fitting procedures, however, can be computationally intensive and time-consuming, especially when dealing with large datasets. To address this limitation, machine learning and deep learning techniques have been explored for FLIM data analysis. When using machine learning techniques for FLIM analysis, two steps are required: image segmentation to identify objects whose parameters need to be evaluated, and determination of the fluorescence decay parameters from data collected during the FLIM measurements. In general, this involves analyzing the fluorescence decay curves to extract information about the properties of the objects. The order of these steps is not strictly defined, but it depends on the specific analysis task and the data available. The conventional procedure for FLIM analysis is presented in Fig. 4.

In our pilot study, we first identified the objects of interest in the FLIM images of liver tissue, which were hepatocytes. We then extracted their parameters. To achieve this, we trained a selected convolutional neural network, modified UNet++ [35], and achieved a high level of cell detection accuracy: the F_1 metric (Dice coefficient) was ~0.7. The results of the image segmentation are presented in Fig. 5.

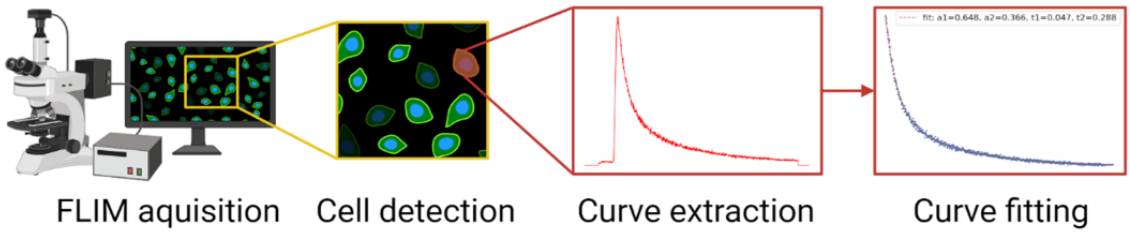

Fig. 4 The procedure for performing FLIM microscopy analysis using machine learning methods.

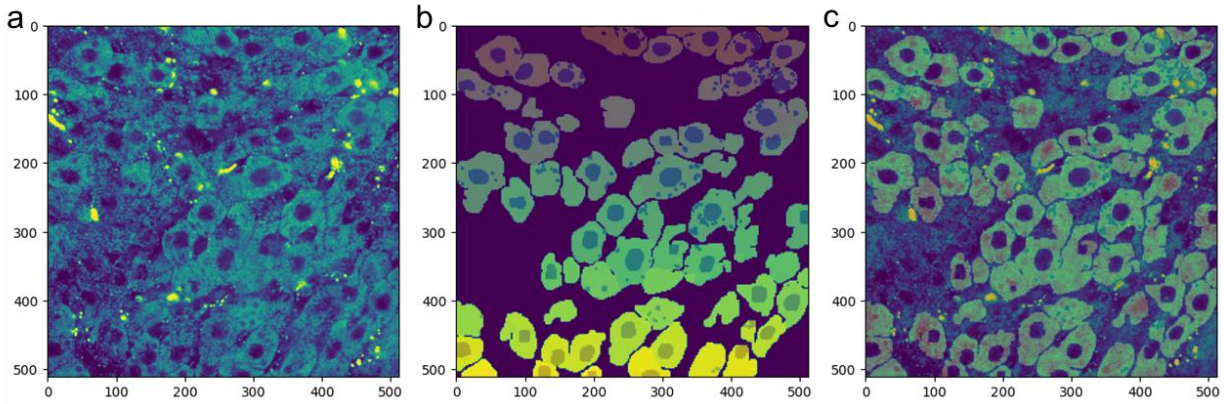

Fig. 5 The results of segmentation of the FLIM image of liver tissue: (a) an intensity image; (b) the resulting cell-by-cell mask, which includes only the cytoplasm of the studied cells; (c) the imposition of a mask on the original image.

3.1 Methods of Biomedical Image Segmentation

Biomedical image is a task that is in demand for the analysis of individual objects in various biomedical images, including the results of laser scanning microscopy, FLIM, magnetic resonance imaging and many other applications. The task of biomedical segmentation has been solved in various ways throughout the development of methods. Early methods assumed direct work with pixels, based on their intensity, color, and mutual arrangement in the image. With the development of deep learning methods, the segmentation task has moved to convolutional neural networks trained for specific segmentation tasks. Now, the most common methods are foundational networks, which are trained on a wide selection of studied images and are suitable for use in various situations. Thus, image segmentation methods are divided into three broad groups: traditional statistical methods, single-task deep learning neural networks and foundational networks.

Traditional statistical machine learning methods for cell image segmentation still are essential tools in biomedical research, allowing for the effective partitioning of cell images into distinct regions for analysis. Thresholding methods, such as Otsu's thresholding, segment images by converting them into binary images based on intensity values. The goal is to find an optimal threshold that separates foreground (cells) from the background. It is commonly used in microscopy to identify and segment cells based on their intensity differences from the background [36]. *K*-Means Clustering partitions the image into k clusters based on pixel intensity or color similarity, effectively grouping similar pixels together. Which is useful for segmenting images where cells exhibit distinct color or intensity profiles [37]. Random Forest is an ensemble learning method that builds multiple decision trees to classify pixels based on features extracted from the image. It is applied in semantic segmentation tasks where each pixel is classified as belonging to a specific cell type or background [38]. Markov Random Fields models spatial dependencies between pixels, allowing for segmentation that considers the relationships between neighboring pixels. It is useful in medical imaging where tissue characteristics vary spatially, helping to manage noise and improve segmentation accuracy [39]. Edge Detection methods, which identify boundaries between different regions by detecting discontinuities in pixel intensity. Common algorithms include Sobel and Canny edge detectors. It is used to delineate cell boundaries in microscopy images, particularly when cells are well-defined against their background [40].

Classical single-task trained deep learning models for cell segmentation have emerged as powerful tools in the analysis of biological images, particularly in identifying and delineating cellular structures. These models leverage deep learning architectures specifically designed for the task of segmenting cells from microscopy images. U-Net is a convolutional neural network architecture specifically designed for biomedical image segmentation. It features a contracting path to capture context and a symmetric expanding path to enable precise localization. U-Net is widely used for segmenting nuclei and other cellular structures in fluorescence microscopy images [41]. DeepCell is a CNN model that focuses on cell segmentation using a patch-based approach. It segments images by classifying each pixel based on learned features from surrounding pixels. It is designed for segmenting diverse cell types in various imaging contexts, including high-throughput microscopy [42]. CellProfiler is not actually an ML model; it uses classical image processing algorithms and can serve as a baseline for comparison with deep learning methods. It employs various modules, including thresholding and shape-based filtering, to identify and segment cells. CellProfiler is frequently used in biological labs for high-throughput image analysis to segment nuclei and other cellular components [43]. SPPNet is designed for nuclei image segmentation and operates with significantly fewer parameters than traditional models while maintaining high performance. It is effective for real-time applications where speed is critical, such as in live-cell imaging scenarios [44]. GeneSegNet integrates gene expression data with imaging information to enhance cell segmentation accuracy. This model employs a recursive training strategy to manage noisy training labels effectively. It is particularly useful in studies involving in situ RNA detection technologies where accurate cell boundaries are crucial for analyzing gene expression data [45].

Foundational models for biomedical image segmentation have evolved significantly, particularly with the advent of deep learning techniques. These models are large-scale pre-trained deep learning models designed to generalize across a variety of tasks with high accuracy, which optimizes the segmentation process and reduces the need for task-specific models.

Many variants of deep learning networks have been developed and modified. One such example is reported in study [46] that describes a new diffusion probabilistic model (DPM) for the medical image segmentation task. Two novel components are introduced in this MedSegDiff approach: a dynamic condition encoder to enhance regional attention in the DPM, and a feature frequency parser to eliminate the negative effects of high-frequency noise components. Experiments on three different datasets demonstrated that the proposed method outperforms existing methods, achieving state-of-the-art results. The authors argue that this is the first time DPM has been used for medical image segmentation.

Research paper [47] introduces a novel neural network architecture designed to overcome the limitations of CNNs and transformers in handling long-range dependencies in medical image segmentation. U-Mamba integrates the local feature extraction capabilities of convolutional layers with the long-term dependency modeling abilities of state space sequence models (SSMs), creating a hybrid CNN-SSM architecture. U-Mamba also has a self-adaptive

mechanism that allows it to automatically adjust to different datasets without the need for manual intervention. This makes it a powerful tool for biomedical image segmentation tasks. There is, however, a paper [48] that introduces a novel approach to medical image segmentation by proposing a U-shape architecture model named Vision Mamba UNet (VM-UNet). This model leverages SSMs to address the limitations of CNN- and transformer-based models. A Visual State Space (VSS) block is introduced to capture extensive contextual information, and an asymmetrical encoder-decoder structure is utilized. VM-UNet is the first medical image segmentation model based solely on SSMs, aiming to set a baseline for more efficient and effective SSM-based segmentation systems in the future.

Another important model is SegMamba [49], which is a novel 3D medical image segmentation model. It effectively captures long-range dependencies within entire volume features at each scale. Compared with transformer-based methods, in whole volume feature modeling SegMamba outperforms these from a state-space model perspective, maintaining superior processing speed even with high-resolution volume features.

In research article [50], the authors propose LM-Net, a lightweight architecture that combines CNNs and Vision Transformers (ViTs) to enhance segmentation accuracy. LM-Net utilizes a multi-branch module to capture multi-scale features and introduces the Local Feature Transformer (LFT) and Global Feature Transformer (GFT) to simultaneously capture local detail textures and global contextual semantics. By integrating these modules, the model achieves state-of-the-art results on various medical image segmentation tasks across different datasets, demonstrating its effectiveness and adaptability.

Paper [51] proposes a semi-supervised contrastive learning framework called ARCO for medical image segmentation. The authors argue that current contrastive learning methods may struggle with distinguishing minority tail-class samples and that this may lead to model collapse. They introduce variance-reduction techniques, which they prove, theoretically, to be universally beneficial for pixel/voxel-level segmentation tasks with limited labels. The authors experimentally validated their approach on eight benchmarks, demonstrating the consistent outperformance of such state-of-the-art semi-supervised methods.

A comparison of the different models is shown in Tables 1 and 2.

Table 1 Comparison table of biomedical image segmentation methods.

Model	Advantages	Limitations
Thresholding [36]	Simple and fast	Sensitive to noise; limited effectiveness with overlapping cells
K-Means [37]	Effective for distinct clusters	Requires predefined *K*; struggles with complex scenes
Random Forest [38]	Robust against overfitting	May lose fine details
Markov Random Fields [39]	Captures spatial relationships	Computationally intensive
Edge Detection [40]	Provides clear boundaries	Affected by noise; may miss edges in smooth areas
U-Net [41]	High accuracy; effective with small datasets	Sensitive to overfitting; requires tuning
DeepCell [42]	Handles complex images well	Computationally intensive
CellProfiler [43]	User-friendly; highly configurable	Lacks accuracy compared to deep learning methods
SPPNet [44]	Fast inference; fewer parameters	May miss contextual details
GeneSegNet [45]	Integrates diverse data; robust against noise	Complexity in data integration
MedSegDiff [46]	State-of-the-art performance; noise reduction	Computationally intensive; sensitive tuning
U-Mamba [47]	Linear complexity; flexible	Requires extensive training data
VM-UNet [48]	Competitive performance; establishes a baseline	Basic architecture without enhancements
SegMamba [49]	Handles complex images; robust performance	High computational demands
LM-Net [50]	Fast inference; lightweight	May sacrifice accuracy in complex scenarios
ARCO [51]	Adaptive region-based segmentation	Implementation complexity; sensitivity issues

Table 2 Comparison table of the application of contemporary biomedical image segmentation methods.

Method	Application
MedSegDiff [46]	General medical image segmentation tasks, particularly where high accuracy is required; effective in segmenting complex anatomical structures across various imaging modalities
U-Mamba [47]	Long-range dependency modeling in segmentation tasks; suitable for tasks requiring detailed contextual understanding, such as organ or tumor segmentation in complex images
VM-Unet [48]	Organ and skin lesion segmentation tasks; effective in scenarios where computational efficiency is crucial without significantly sacrificing accuracy
SegMamba [49]	Complex images with overlapping structures; suitable for challenging segmentation tasks where traditional methods may struggle, such as in dense tissue imaging
LM-Net [50]	Real-time medical image segmentation tasks; suitable for applications requiring rapid processing, such as intraoperative imaging or point-of-care diagnostics
ARCO [51]	Adaptive region-based segmentation tasks; effective in segmenting heterogeneous regions, such as differentiating between various tissue types in medical scans

Table 3 Comparison table of various accuracy metrics for image segmentation methods.

Model	Mean IoU	Pixel Acc	Dice
MedSegDiff [46]	0.807		0.882
U-Mamba [47]			0.6964
VM-Unet [48]	0.8079	0.956	0.8937
SegMamba [49]	0.8859		0.6967
LM-Net [50]	0.8912		0.9409
ARCO [51]			0.852

3.2 Image Segmentation Quality Metrics

In the field of computer vision, accurate segmentation metrics are essential tools for evaluating segmentation models. These metrics provide quantitative measurements that assess how well the model separates objects in an image. They allow developers to evaluate the effectiveness of the model, identify weaknesses, and make improvements. There are several metrics available, such as Pixel Accuracy, Mean Intersection over Union (mIoU), and Dice Coefficient. Each metric provides unique insights into the performance of the model for different applications and challenges [52]:

- mAP (mean Average Precision) and AR (Average Recall) metrics to assess base accuracy.
- Dice, mIoU (Jaccard) to evaluate the mask accuracy.
- Precision and Recall to assess classification correctness.
- Confusion Matrix, per-class and per-image metrics to get more insights regarding the instance segmentation model.

A comparison of the different models based on the indicators presented is shown in Table 3.

Challenges remain, however, particularly in handling the complexity of clinical tissue samples and the large size of whole-slide images. The difficulties of segmenting abnormal tissues in medical images, such as the heterogeneity of tumor morphology and the need to process gigapixel-scale images, remains [53, 54].

Overall, the field of tissue image segmentation has seen significant progress, driven by advances in deep learning, the creation of large annotated datasets, and innovative algorithmic approaches. However, continued research is needed to address the unique challenges posed by clinical tissue samples and to enable more accurate and efficient analysis of these critical medical images.

3.3 Curve Analysis

The FLIM decay parameters, as mentioned above, are calculated on the basis of the approximation of the decay curve, for each pixel or selected field, with further parameter estimation depending on the resulting function. Thus, the basic approach to conducting FLIM analysis is curve fitting.

Curve fitting is a fundamental tool in data analysis and modelling, used across various disciplines to describe and predict relationships between variables. Curve fitting involves finding a mathematical function that best fits a set of data points. The goal is to capture the underlying trend or pattern in the data, allowing for

interpolation, extrapolation, and prediction. Commonly used functions for curve fitting include linear, polynomial, exponential, logarithmic, and trigonometric functions.

3.4 Techniques for Curve Fitting

There are several standard curve fitting methods that include: linear regression, nonlinear regression, polynomial functions, and splines. These techniques have been used to analyze curves with great efficiency for a long time and do not require further explanation [55−58].

Machine learning offers powerful techniques for curve fitting, including neural network and deep learning approaches. These methods provide flexibility in capturing complex, nonlinear relationships compared to traditional polynomial regressions.

Indeed, neural networks excel at function approximation, making them well-suited for curve fitting problems. By using a sufficient number of hidden layers and neurons, neural networks can learn to fit arbitrary curves to data. The key is to train the network on the dataset, allowing it to learn the underlying function. One approach is to use an extreme learning machine (ELM) algorithm, which introduces an additional linear neuron to correct the output of the hidden layer neurons. The number of hidden neurons is optimized using particle swarm optimization (PSO) to achieve the best fit. This method has shown excellent performance on various benchmark datasets and real-world applications [59].

Deep learning architectures, such as deep neural networks with multiple hidden layers, offer even more flexibility in curve fitting. By stacking multiple nonlinear transformations, deep networks can capture highly complex relationships in the data. This is particularly useful when fitting curves to high-dimensional or multivariate datasets. For example, convolutional neural networks can be applied to curve fitting problems by treating the input data as an image-like structure. The convolutional layers extract relevant features, while the fully connected layers perform the actual curve fitting. This approach has been demonstrated on multidimensional curve fitting tasks [60].

Machine learning and deep learning methods provide a number of advantages for curve fitting compared to traditional methods. Neural networks and deep learning models can match a wide range of curve shapes, including highly nonlinear and complex functions. They can automatically extract relevant functions from data, without the need for manual function design, are suitable for fitting curves to large-dimensional datasets such as those used in scientific and engineering applications, and can be trained to be resistant to noise and outliers in the data, providing reliable curve fitting results. With powerful computing resources and large datasets, machine learning methods can scale to fit curves to massive datasets.

Despite the promising results of machine learning and deep learning in the field of curve fitting, there are still challenges and areas that require improvement. One such main issue is interpreting the fitted curves produced by the deep learning models. This is particularly challenging for high-dimensional problems, where it can be difficult to understand the underlying patterns. Ensuring that the fitted curves generalize well to new data is crucial for the success of these models. Techniques such as regularization and cross-validation can help to improve such generalizations, but more research is needed in this area. Another important aspect of curve fitting is obtaining reliable estimates of uncertainty. Combining traditional curve fitting methods with machine learning techniques, such as spline interpolation or Bayesian approaches, can lead to more accurate and reliable results.

3.5 Contemporary Premade Curve Fitting Solutions

There are many premade solutions for analyzing curves, in particular, fluorescence attenuation curves, thanks to which you can quickly select the parameters of the decay curve function and obtain calculated decay parameters.

Research paper [61] introduces CurvPy, an open-source Python library designed for automated curve fitting and regression analysis. CurvPy aims to make advanced statistical and machine learning techniques more accessible by providing functionalities for optimization, smoothing, imputation, summarization, visualization, regression, evaluation, and tuning. The methodology of CurvPy involves the use of mathematical techniques such as least squares estimation, Savitzky-Golay filtering, matrix completion, gradient descent optimization, regularization, basis function regression, and standard model evaluation metrics. This highlights the contributions of CurvPy in simplifying model fitting and analysis for both non-experts and power users, emphasizing usability, flexibility, and transparency in leveraging advanced statistical methods for data analysis.

Research paper [62] describes TableCurve 2D a powerful software tool for automated curve fitting and data modeling, widely used by engineers and scientists. It offers a range of features that make it a valuable tool for analyzing data. One of the key features of TableCurve 2D is its ability to automatically fit curves to data using a library of 3,665 equations. This saves time and effort compared to manual fitting, as users can quickly find the best fit with a single click. Additionally, users can define up to 15 custom equations for more complex modeling needs. TableCurve also provides advanced estimation procedures for nonparametric models, such as Spline, Smoothing Spline, and Local Regression. These methods are useful for data that does not fit well within traditional parametric models.

Wolfram Language, introduced in Ref. [63], offers powerful tools for curve fitting, supporting both linear and nonlinear approaches. Users can quickly approximate data with linear least-squares regression using specified basis functions, while nonlinear models allow for more flexibility with constraints and initial parameter estimates. Interpolation methods are also

available to create smooth curves that pass-through data points, without assuming a specific functional form. Regularization techniques prevent overfitting by penalizing large coefficient values, and diagnostic tools help assess fit quality with statistical measures. These capabilities are useful in various fields, such as physics for modeling experimental data, biology for growth or decay curve fitting, and engineering for stress-strain analysis.

A further paper [64] introduces ndCurveMaster, an example of curve fitting software, providing tools for automated curve fitting, managing unlimited variables, and heuristic techniques for optimal fitting, together with advanced statistical analysis tools such as Analysis of Variance (ANOVA), regression analysis, and overfitting detection. The software's integration of machine learning techniques for equation discovery significantly enhances the efficiency of data analysis, and its extensive applicability across disciplines such as medicine, physics, ecology, and finance.

In addition to the listed options for premade methods for analyzing decay curves there another options including open-source and programming languages-based methods, which is important to mention.

ImageJ [65], a popular open-source image processing software, offers several tools for decay curve fitting, particularly useful in fluorescence lifetime imaging and other applications where analyzing decay kinetics is essential. FILMJ is an advanced ImageJ toolkit specifically designed for fluorescence lifetime data analysis. It integrates seamlessly with the ImageJ Ops framework and includes various fitting routines that can be extended for complex workflows. FILMJ supports standard nonlinear least-squares fitting using the Levenberg-Marquardt algorithm, as well as more sophisticated methods like maximum likelihood and Bayesian analysis.

Gwyddion [66] is a powerful open-source software for analyzing and processing data from scanning probe microscopy (SPM) and other imaging techniques. It includes various tools for curve fitting, particularly useful for decay curve fitting in the context of surface roughness and force-distance data analysis. Gwyddion employs the Levenberg-Marquardt algorithm for nonlinear curve fitting, which is suitable for statistical functions used in evaluating surface roughness parameters. The software provides a range of fitting functions, including Gaussian and exponential models, which can be applied to various datasets, including those derived from AFM measurements.

Python, alongside other programming languages-based methods, like MATLAB or R-Studio, is a powerful tool for decay curve fitting, particularly using special libraries such as SciPy and NumPy for Python. It allows users to define custom functions for fitting, enabling them to model a wide range of decay behaviors tailored to specific datasets. Libraries like SciPy provide built-in functions, which simplifies the process of fitting data to models using nonlinear least squares optimization.

4 Complex Analysis of Obtained FLIM Data Using Machine Learning

Machine learning techniques are well-suited to extracting and interpreting measurements from multi-dimensional FLIM data sets, offering significant improvements in the efficiency of data analysis. FLIM data extraction using curve-fitting techniques can be complex and computationally inefficient for real-time measurements, especially in applications like FRET that require analysis in multiple dimensions. Machine learning approaches can accelerate imaging processes, aid in data interpretation, and extract multi-dimensional data into a single exponent lifetime, addressing the challenges faced by traditional curve-fitting methods. In the context of metabolic imaging, machine learning models can be trained to map FLIM imaging data to provide target outputs, such as metabolic states or the presence of biomarkers [67].

The diverse approaches to deep learning, which are tailored to process raw FLIM data, encompass physics-based models. Physics-based deep learning (PBDL) models integrate fundamental physical principles into machine learning frameworks to enhance performance in various applications, including fluorescence lifetime imaging.

4.1 State-of-the-Art Methods of FLIM Data Analysis

Research paper [11] introduces a deep learning approach called FLI-Net which is proposed as a fit-free method for FLIM image formation that can quantify fluorescence decays simultaneously over a whole image at high speed. FLI-Net has a deep neural network architecture designed and trained for different classes of experiments, including visible FLI, near-infrared (NIR) FLIM, and NIR gated Macroscopy Fluorescent Lifetime Imaging (MFLI). FLI-Net outputs the spatially resolved lifetime-based parameters typically employed in the field, without requiring any parameter settings. The paper [68] presents AUTO-FLI, a groundbreaking deep learning framework for three-dimensional fluorescence lifetime tomography that significantly enhances accuracy and computational efficiency. By employing a two-stage convolutional neural network architecture, consisting of modified Automap and modified FLI-Net, AUTO-FLI achieves highly accurate reconstructions of three-dimensional intensity and lifetime distributions from raw two-dimensional fluorescence decays, outperforming conventional methods. The use of Monte-Carlo Xtreme for data generation reduces the time and resources required for training, making the model more robust and versatile across a wide range of biological and medical imaging applications.

Another research paper [69] introduces a deep learning framework called Few-Photon Fluorescence Lifetime Imaging (FPFLI), designed for analyzing FLIM data under low-light conditions with minimal photons per pixel. Traditional FLIM analysis methods struggle with low photon counts, requiring hundreds to thousands of

photons for accurate results. FPFLI breaks away from pixel-wise analysis, leveraging spatial correlation and intensity information to estimate lifetime images effectively with only a few photons. The framework involves two main steps: estimating local lifetime distributions using a Local Lifetime Estimator (LLE) and fusing this information with intensity images to reconstruct target lifetime images using Neural Implicit Image Interpolation (NIII). The study includes the development of a large-scale synthetic FLIM dataset for training the FPFLI algorithm, demonstrating rapid and robust lifetime estimation even with extremely low photon counts. The paper outlines the algorithm's implementation, training process, and evaluation using semi-synthetic FLIM datasets to overcome challenges in acquiring diverse FLIM images for training the deep learning algorithms.

Paper [70] introduces a compact deep learning architecture called Fluorescence Life-time AdderNet (FLAN) for high-fidelity FLIM imaging with low computing overheads. FLAN is designed for efficient implementation on field-programmable gate arrays (FPGA), aiming to improve the performance of FLIM while reducing computational complexity. The architecture uses an adder-based deep learning network that avoids multiplication-based convolutions, simplifying calculations and making it more suitable for real-time applications with limited computational resources. The network employs a log-scale (LS) merging technique to compress fluorescence decay data, achieving significant compression ratios of 0.11 and 0.23 compared to traditional convolutional neural networks, while maintaining high accuracy in lifetime retrieval. This architecture has been successfully implemented on FPGA, using post-quantization techniques to optimize computational efficiency and minimize resource usage. The implementation allows for high performance in real-time biomedical research applications. Evaluations on synthetic and experimental FLIM data show that FLAN and FLAN+LS achieve state-of-the-art accuracy and precision, outperforming traditional curve fitting methods, especially in low photon count conditions. Finally, the paper demonstrates real-time FLIM imaging by implementing FLAN+LS on an FPGA, achieving high throughput by processing multiple pixels in parallel.

Another paper [71] discusses a hardware-friendly deep learning architecture utilizing one-dimensional convolutional neural networks (1D CNN) for analyzing FLIM data. This architecture highlights the advantages of 1D CNNs over high-dimensional CNNs, emphasizing their simplicity, faster training, and quicker processing speeds. Notably, 1D CNNs excel in handling multi-exponential fluorescence decay models and have shown superior performance in fluorescence lifetime image reconstruction compared to traditional LS methods, particularly validated when using simulated data. The authors also mention the successful application of the proposed 1D CNN in analyzing two-photon FLIM images of functionalized gold nanoprobes in Hek293 and human prostate cancer cells, showcasing the speed and accuracy of 1D CNNs in extracting lifetime parameters from fluorescence signals. Overall, the study underscores the significant potential of 1D CNNs in real-time FLIM applications.

Paper [72] introduces a deep learning architecture model, the MLP-Mixer, that can perform fast and accurate fluorescence lifetime imaging. Compared to other methods like 1D-CNN, NLSM, and VPM, the MLP-Mixer model achieves the best performance in terms of low bias and small standard deviation, together with high correlation with the reference lifetimes for both Rhodamine B and Rhodamine 6G samples across different signal-to-noise ratios. The MLP-Mixer model has a simple architecture and fewer parameters compared to the 1D-CNN model, yet it outperforms the 1D-CNN in both training time and inference time. This makes the MLP-Mixer a practical and efficient solution for real-time fluorescence lifetime imaging applications. The paper demonstrates the effectiveness of the proposed deep learning approach through both simulation and experimental results using Rhodamine 6G, Rhodamine B, and Convallaria majalis cell samples. The results show that such deep learning models can more accurately estimate fluorescence lifetimes compared to traditional methods like nonlinear LS fitting.

Paper [73] introduces FlimGANE, a fluorescence lifetime imaging method based on Generative Adversarial Network Estimation. It consists of a generator, a discriminator, and an estimator, with the generator using convolutional and residual blocks to generate high-quality decays from low-photon-count inputs. The discriminator is composed of fully connected layers, and the estimator involves training with mean-squared error cost functions. FlimGANE is trained in three stages: generative model training, estimative model training, and combination training. It addresses the need for a computationally efficient and high-quality method for fluorescence lifetime estimation, performing well even in ultra-low-photon-count conditions. It outperforms traditional methods like TD-MLE in barcode identification, FRET characterization, and metabolic state analysis, offering a reliable alternative for FLIM analyses, especially in clinical applications like retinal imaging and tumor margin identification.

The article [74] discusses advancements in time-domain diffuse optical tomography (TD-DOT), particularly focusing on a new reconstruction algorithm called SENSOR-NET. This technology aims to enhance the clinical application of TD-DOT for monitoring brain tissue hemodynamics by providing high spatial and temporal resolution. TD-DOT offers superior accuracy in measuring optical properties and physiological parameters compared to frequency-domain or steady-state methods.

However, it faces challenges in achieving high temporal resolution due to the computational demands of solving the inverse problem, which can lead to long reconstruction times. The authors introduce the SENSOR algorithm, which is a non-iterative approach that significantly reduces computation time while maintaining high spatial resolution (1 mm) and temporal

resolution (20−30 ms). This algorithm transforms the complex inverse problem into a more manageable format, allowing for faster processing without iterative solving. The proposed SENSOR-NET integrates deep learning with the SENSOR algorithm. By structuring the iterations of SENSOR within a neural network, SENSOR-NET eliminates the need for empirical parameter tuning prior to reconstruction. Once trained, this model can achieve accurate reconstructions in under 20 ms, independent of the number of sources or wavelengths used. The method has been validated using both numerical simulations and experimental data, demonstrating its potential for real-time brain monitoring and other applications requiring rapid imaging capabilities.

Another paper [75] introduces a Bayesian Nonparametric FLIM (BNP-FLIM) is an innovative framework designed to enhance fluorescence lifetime imaging microscopy by addressing key challenges in quantitative analysis. Traditional FLIM methods often ignore spatial correlations between pixels, rely on photon ratios instead of absolute lifetime maps, and struggle to determine the number of contributing fluorophore species. BNP-FLIM overcomes these issues by employing a doubly nonparametric approach that uses Beta-Bernoulli process priors to [infer the number of species and Gaussian process priors for continuous lifetime mapping.

This framework leverages information from "empty pulses" − pulses that do not result in observable photons − to improve lifetime estimates. Benchmarking against synthetic and experimental data demonstrates its robustness, allowing for the recovery of lifetime differences as small as 0.3 ns with only 1000 photons. BNP-FLIM significantly enhances spatial resolution and enables rigorous uncertainty propagation.

Thus, the use of machine learning in complex FLIM imaging analysis aligns with its broader applications in medical imaging, where it plays a crucial role in tasks like disease diagnosis, characterization, and treatment response prediction [76].

A comparison of the methods of FLIM data complex analysis is shown in Table 4 and 5.

Methods available on GitHub are listed in Table 6.

Table 4 Comparison table of the application of various methods of FLIM data complex analysis.

Method	Application
FLI-Net [11]	Rapid analysis of fluorescence lifetime imaging data; effective for tasks requiring fast processing, such as monitoring dynamic biological processes or detecting changes in fluorescence lifetimes in live cells
FPFLI [69]	Advanced fluorescence lifetime imaging with enhanced sensitivity; suitable for high-resolution imaging tasks where detailed analysis of molecular interaction is required
FLAN [70]	Analyzing complex datasets with multiple parameters; suitable for studies involving microenvironmental changes or interactions among multiple fluorescent species
1D CNN [71]	Fast processing of sequential fluorescence data; effective for real-time analysis of time-series data in flim applications, particularly in simple scenarios where spatial features are less critical
MLP-Mixer [72]	General-purpose application requiring efficient processing of sequence signals; suitable for various flim applications, especially where speed and accuracy are essential, such as in embedded systems or real-time imaging
FlimGANE [73]	Enhancing image quality and resolution in fluorescence lifetime imaging; useful for improving the quality of fluorescence lifetime maps, especially under low-photon conditions or when dealing with challenging imaging scenarios
SENSOR-Net [74]	Simultaneous learning of fluorophore species and their absolute lifetime maps while leveraging spatial correlations; effective for characterizing complex biological environments by providing high-resolution lifetime maps while accounting for uncertainties inherent in experimental data
BNP-FLIM [75]	Overcoming challenges in quantitative flim analysis by learning the number of species and their absolute lifetime maps simultaneously; suitable for scenarios where distinguishing between closely spaced lifetimes is critical, such as drug discovery and monitoring biological interactions

Table 5 Comparison table of various methods of FLIM data complex analysis.

Method	Advantages	Limitations
FLI-Net [11]	High accuracy in quantifying fluorescence lifetimes; approximately 30 times faster than traditional methods like spcimage; well-suited for real-time analysis in complex biological samples	The outcome may vary depending on the unique properties of the sample being examined; to attain the best results, it may be necessary to have a substantial amount of training data
FPFLI [69]	Enhanced fluorescence lifetime imaging capabilities; provides improved sensitivity and resolution compared to traditional methods	May be complex to implement and require specialized hardware; performance can vary depending on the imaging setup and sample conditions
FLAN [70]	Designed for efficient analysis of fluorescence lifetime data; capable of handling complex datasets with multiple parameters	Implementation may be challenging without adequate computational resources; require careful calibration to ensure accurate results
1D CNN [71]	Efficient for processing sequential data, suitable for time-series analysis in fluorescence imaging; simple architecture that can be trained quickly on smaller dataset	Limited ability to capture spatial features compared to 2D or 3D cnns; may not perform as well on complex imaging tasks requiring detailed spatial context
MLP-Mixer [72]	Offers simplicity, flexibility, and scalability; performs well on large datasets while being computationally efficient	Limited interactions with neighboring neurons can result in decreased performance with smaller datasets; still relatively new with less established performance metrics in specific biomedical applications
FlimGANE [73]	Combines gans with fluorescence lifetime imaging to enhance image quality and resolution rapidly, even under low-photon conditions; up to 2800 times faster than traditional maximum likelihood estimation methods while providing accurate analyses	Training gans can be resource-intensive and time-consuming; performance may be affected by the stability of the photon-counting electronics used in imaging setup
SENSOR-Net [74]	Leverages spatial correlations and empty pulse information for robust analysis; dynamically learns the number of species and their corresponding lifetime maps simultaneously	Requires sophisticated mathematical modeling and understanding of bayesian methods; may demand significant computational power for processing large datasets
BNP-FLIM [75]	Learns the number of species and their absolute lifetime maps without prior assumptions about species count; effectively propagates uncertainties across species and lifetime estimates	The bayesian framework can be computationally intensive due to the complexity of the models used; requires high-quality data to ensure accurate modeling and predictions

Table 6 Table of various methods available on GitHub.

Model	GitHub
MedSegDiff [46]	https://github.com/SuperMedIntel/MedSegDiff.git, 21 Jan 2025
U-Mamba [47]	https://github.com/bowang-lab/U-Mamba.git, 21 Jan 2025
VM-Unet [48]	https://github.com/JCruan519/VM-UNet.git, 21 Jan 2025
SegMamba [49]	https://github.com/ge-xing/SegMamba.git, 21 Jan 2025
LM-Net [50]	https://github.com/Asunatan/LM-Net.git, 21 Jan 2025

Table 6 Cont.

ARCO [51]	https://github.com/charlesyou999648/ARCO.git, 21 Jan 2025
FLI-Net [11]	https://github.com/jasontsmith2718/DL4FLI.git, 21 Jan 2025
FPFLI [69]	https://github.com/Dooongx/FPFLI.git, 21 Jan 2025
FlimGANE [73]	https://github.com/NinaYIC/flimGANE.git, 21 Jan 2025
BNP-FLIM [75]	https://github.com/MohamadFazel/BNP2-FLIM.git, 21 Jan 2025

4.2 Advantages and Limitations of ML in FLIM

Machine learning (ML) techniques can provide more accurate estimates of fluorescence lifetimes and metabolic pathways compared to traditional analysis methods. ML algorithms can also analyze fluorescence lifetime imaging (FLIM) data faster, allowing for real-time decision-making and analysis. This enables a more intuitive understanding of the data, providing insights into cellular metabolism and disease progression. Label-free imaging combined with ML removes the need for time-consuming and expensive labeling processes, making this approach a powerful tool for researchers. ML can handle complex multi-dimensional FILM data, extracting valuable information that can be used to improve clinical outcomes. However, implementing ML in FILM requires large and high-quality datasets, as well as appropriate approaches to overcoming clinical, professional, and technical challenges to its successful translation to clinical practice [77]. There are many techniques for the denoising of FLIM images using machine learning and deep-learning methods.

5 Future Directions

Physics-based deep learning (PBDL) is an emerging approach that combines the principles of physics with deep learning algorithms to enhance the performance, effectiveness, and resilience of various applications. In the context of FLIM, the potential of PBDL in overcoming the constraints of conventional data-driven or physics-based methods is immense. However, there are no existing PBDL models tailored specifically for FLIM yet.

PBDL models leverage governing equations, such as partial differential equations, by embedding them into the architecture or loss functions, promoting solutions that adhere to known physics. By incorporating physical laws, PBDL models achieve high accuracy with less training data, making them particularly beneficial in scenarios where large datasets are challenging to obtain. They effectively address both forward simulations and inverse problems, allowing for a wide range of applications. The augmentation of loss functions with physical constraints ensures that predictions align with real-world behaviors, while differentiable physics simulations enable tight coupling between deep learning and physical modeling. Additionally, PBDL models can utilize virtual data points to evaluate physical consistency, enhancing training efficiency. In FLIM and beyond, these models improve analysis by providing robust, physically consistent solutions that are resilient to noise and variability, making them valuable tools for real-time assessments and dynamic process monitoring in scientific research and practical applications [78−80].

The integration of physical constraints, such as models of fluorescence decay and photon transport, into deep learning architectures is a significant advancement in the field of FLIM. One way to effectively embed physical constraints is by integrating governing equations related to fluorescence decay and photon transport into the loss function of deep learning models. Using partial differential equations (PDEs) as regularizers guides the training process, ensuring that model predictions adhere to known physical laws. Physics-Informed Neural Networks (PINNs) are neural networks designed to solve forward and inverse problems involving nonlinear PDEs, incorporating physical laws directly into their architecture. These networks can learn from limited data while ensuring physically plausible predictions, which is particularly useful in FLIM where data can be scarce or noisy. Recent advancements have led to the introduction of filtered PDEs as surrogate constraints within PBDL frameworks. This approach enables robust solutions even in noisy environments, by calculating PDE losses based on filtered variables. It maintains the integrity of the governing equations, while being less sensitive to noise. Simulated datasets, based on known physical models, can augment real experimental data, providing additional training examples for deep learning models. This improves the model's ability to generalize across different experimental conditions, enhancing its performance [11, 81, 82].

Developing models that effectively integrate deep learning with physical simulations can be complex and requires a deep understanding of both fields. This complexity may limit accessibility for practitioners who are not experts in either domain. While PBDL reduces the need for large datasets, the quality of the available data remains critical. Poor quality or biased data can lead to inaccurate models, undermining the benefits of integrating physical knowledge. Training hybrid models that combine deep learning with physics-based simulations often requires significant computational resources, which may not be available to all researchers or institutions [78−80].

As this field continues to develop, overcoming the challenges of integration and computational demands will be crucial for unlocking the full potential of PBDL

in FLIM applications. This will ultimately advance our understanding of complex biological systems.

6 Conclusion

The review summarizes recent advances in the use of machine learning and deep learning techniques for fluorescence lifetime imaging microscopy data analysis and modeling.

An analysis of the use of deep learning methods for FLIM data analysis showed that:

- FLI-Net, 1D CNN, MLP-Mixer are suitable for real-time FLIM;
- FPFLI, FlimGANE are suitable for low-photon conditions;
- FLAN is suitable for FPGA;
- SENSOR-Net, BNP-FLIM are suitable for simultaneous FLIM estimation and classification;
- FPFLI, FlimGANE, SENSOR-Net and BNP-FLIM are suitable for high-resolution imaging;
- FLI-Net, MLP-Mixer, FlimGANE and especially BNP-FLIM are significant resistant to data noise;
- FLI-Net, FPFLI and FlimGANE are suitable for small datasets.

Traditional methods for extracting fluorescence lifetimes from FLIM data can be complex and time-consuming, but machine learning and deep learning approaches have emerged as promising alternatives that offer faster and more accurate lifetime extraction.

Convolutional neural networks have been particularly prevalent in FLIM analysis, demonstrating effectiveness in denoising and enhancing fluorescence microscopy images, as well as in developing novel techniques.

In conclusion, machine learning and deep learning-based techniques have demonstrated great potential in FLIM data modeling, offering faster and more accurate lifetime extraction, denoising capabilities, and improved image enhancement.

Funding

Russian Science Foundation №23-15-00100.

Acknowledgment

Thanks to Svetlana Rodimova, Daria Kuznetsova and Vladislav Shcheslavsky (PRMU) for their help in writing the manuscript.

Disclosures

The authors declare no conflicts of interest.

Data Availability

No data were generated or analyzed in the presented research.

References

1. R. Datta, T. M. Heaster, J. T. Sharick, A. A. Gillette, and M. C. Skala, "Fluorescence lifetime imaging microscopy: fundamentals and advances in instrumentation, analysis, and applications," Journal of Biomedical Optics 25(07), 1 (2020).
2. P. A. Bonilla, R. Shrestha, "FLIM-FRET Protein-Protein Interaction Assay," in KRAS, A. G. Stephen and D. Esposito (Eds.), 2797, Springer US, 261–269 (2024).
3. P. P. Provenzano, K. W. Eliceiri, and P. J. Keely, "Multiphoton microscopy and fluorescence lifetime imaging microscopy (FLIM) to monitor metastasis and the tumor microenvironment," Clinical & Experimental Metastasis 26(4), 357–370 (2009).
4. S. Karpf, C. T. Riche, D. Di Carlo, A. Goel, W. A. Zeiger, A. Suresh, C. Portera-Cailliau, and B. Jalali, "Spectro-temporal encoded multiphoton microscopy and fluorescence lifetime imaging at kilohertz frame-rates," Nature Communications 11(1), 2062 (2020).
5. M. Evers, N. Salma, S. Osseiran, M. Casper, R. Birngruber, C. L. Evans, and D. Manstein, "Enhanced quantification of metabolic activity for individual adipocytes by label-free FLIM," Scientific Reports 8(1), 8757 (2018).
6. T. Sanchez, T. Wang, M. V. Pedro, M. Zhang, E. Esencan, D. Sakkas, D. Needleman, and E. Seli, "Metabolic imaging with the use of fluorescence lifetime imaging microscopy (FLIM) accurately detects mitochondrial dysfunction in mouse oocytes," Fertility and Sterility 110(7), 1387–1397 (2018).
7. W. Becker, A. Bergmann, L. Braun, and Becker, "Metabolic Imaging with the DCS-120 Confocal FLIM System : Simultaneous FLIM of NAD (P) H and FAD," Application note (2018).
8. A. D. Komarova, S. D. Sinyushkina, I. D. Shchechkin, I. N. Druzhkova, S. A. Smirnova, V. M. Terekhov, A. M. Mozherov, N. I. Ignatova, E. E. Nikonova, E. A. Shirshin, L. E. Shimolina, S. V. Gamayunov, V. I. Shcheslavskiy, and M. V. Shirmanova, "Insights into metabolic heterogeneity of colorectal cancer gained from fluorescence lifetime imaging," eLife 13, RP94438 (2024).
9. Y. Ouyang, Y. Liu, Z. M. Wang, Z. Liu, and M. Wu, "FLIM as a Promising Tool for Cancer Diagnosis and Treatment Monitoring," Nano-Micro Letters 13(1), 133 (2021).
10. B. W. Weyers, M. Marsden, T. Sun, J. Bec, A. F. Bewley, R. F. Gandour-Edwards, M. G. Moore, D. G. Farwell, and L. Marcu, "Fluorescence lifetime imaging for intraoperative cancer delineation in transoral robotic surgery," Translational Biophotonics 1(1–2), e201900017 (2019).

11. J. T. Smith, R. Yao, N. Sinsuebphon, A. Rudkouskaya, N. Un, J. Mazurkiewicz, M. Barroso, P. Yan, and X. Intes, "Fast fit-free analysis of fluorescence lifetime imaging via deep learning," Proceedings of the National Academy of Sciences 116(48), 24019–24030 (2019).
12. A. Buades, B. Coll, and J.-M. Morel, "A review of image denoising algorithms, with a new one," Multiscale Modeling and Simulation 4 (2), 490–530 (2005).
13. A. Shah, J. I. Bangash, A. W. Khan, I. Ahmed, A. Khan, A. Khan, and A. Khan, "Comparative analysis of median filter and its variants for removal of impulse noise from gray scale images," Journal of King Saud University-Computer and Information Sciences 34(3), 505–519 (2022).
14. W. Zhou, Y. Miura, "Denoising method using a moving-average filter for the moving-object recognition of low-illuminance video-image," in 2016 IEEE International Conference on Consumer Electronics-Taiwan (ICCE-TW), IEEE (2016).
15. D. Bhonsle, V. Chandra, and G. R. Sinha, "Medical Image Denoising Using Bilateral Filter," International Journal of Image, Graphics and Signal Processing 4(6), 36–43 (2012).
16. S. Shrestha, "Image Denoising using New Adaptive Based Median Filters," Signal & Image Processing: An International Journal (SIPIJ) 5(4), 1−13 (2014).
17. Z. Shan, J. Yang, M. A. F. Sanjuán, C. Wu, and H. Liu, "A novel adaptive moving average method for signal denoising in strong noise background,"The European Physical Journal Plus 137(1), 50 (2022).
18. R. Tian, G. Sun, X. Liu, and B. Zheng, "Sobel Edge Detection Based on Weighted Nuclear Norm Minimization Image Denoising," Electronics 10(6), 655 (2021).
19. B. Jakisc, R. Ivokovic, B. Gara, M. Petrovic, and P. Spalevic, "Analysis of different influence of compression algorithm on the image filtered Laplacian, Prewitt and Sobel operator," International Journal of Darshan Institute on Engineering Research & Emerging Technologies 2(1), 68–76 (2013).
20. W. Piao, Y. Yuan, and H. Lin, "A Digital Image Denoising Algorithm Based on Gaussian Filtering and Bilateral Filtering," ITM Web of Conferences 17, 01006 (2018).
21. S. Paris, S. W. Hasinoff, and J. Kautz, "Local Laplacian filters: edge-aware image processing with a Laplacian pyramid," Communications of the ACM 58(3), 81–91 (2015).
22. Y. Raphiphan, S. Wattanakaroon, and S. Khetkeeree, "Adaptive High Boost Filtering for Increasing Grayscale and Color Image Details," in 2020 International Conference on Power, Energy and Innovations (ICPEI), IEEE, 69–72 (2020).
23. Z. Shi, Y. Chen, E. Gavves, P. Mettes, and C. G. M. Snoek, "Unsharp Mask Guided Filtering," IEEE Transactions on Image Processing 30, 7472–7485 (2021).
24. M. A. Digman, V. R. Caiolfa, M. Zamai, and E. Gratton, "The phasor approach to fluorescence lifetime imaging analysis," Biophysical Journal 94(2), L14–L16 (2008).
25. V. Mannam, Y. Zhang, X. Yuan, T. Hato, P. C. Dagher, E. L. Nichols, C. J. Smith, K. W. Dunn, and S. Howard, "Convolutional neural network denoising in fluorescence lifetime imaging microscopy (FLIM)," in Multiphoton Microscopy in the Biomedical Sciences XXI, A. Periasamy, P. T. So, and K. König (Eds.), SPIE Proceedings 11648, 116481C (2021).
26. B. Fu, X. Zhao, Y. Li, X. Wang, and Y. Ren, "A convolutional neural networks denoising approach for salt and pepper noise," Multimedia Tools and Applications 78, 30707–30721 (2019).
27. P. C. Tripathi, S. Bag, "CNN-DMRI: A Convolutional Neural Network for Denoising of Magnetic Resonance Images," Pattern Recognition Letters 135, 57–63 (2020).
28. Y. Kim, J. W. Soh, G. Y. Park, and N. I. Cho, "Transfer Learning from Synthetic to Real-Noise Denoising with Adaptive Instance Normalization," in Proceedings of the IEEE/CVF Conference on Computer Vision and Pattern Recognition, 3482–3492 (2020).
29. V. Kapitany, A. Fatima, V. Zickus, J. Whitelaw, E. McGhee, R. Insall, L. Machesky, and D. Faccio, "Single-sample image-fusion upsampling of fluorescence lifetime images," Science Advances 10(21), eadn0139 (2024).
30. C. Callenberg, A. Lyons, D. D. Brok, A. Fatima, A. Turpin, V. Zickus, L. Machesky, J. Whitelaw, D. Faccio, and M. B. Hullin, "Super-resolution time-resolved imaging using computational sensor fusion," Scientific Reports 11, 1689 (2021).
31. B. Huang, J. Li, B. Yao, Z. Yang, E. Y. Lam, J. Zhang, W. Yan, and J. Qu, "Enhancing image resolution of confocal fluorescence microscopy with deep learning," PhotoniX 4, 2 (2023).
32. D. Xiao, Z. Zang, W. Xie, N. Sapermsap, Y. Chen, and D. D. Uei Li, "Spatial resolution improved fluorescence lifetime imaging via deep learning," Optics Express 30(7), 11479 (2022).
33. M. Adhikari, R. Houhou, J. Hniopek, and T. Bocklitz, "Review of Fluorescence Lifetime Imaging Microscopy (FLIM) Data Analysis Using Machine Learning," Journal of Experimental and Theoretical Analyses 1(1), 44–63 (2023).
34. W. Shi, D. E. S. Koo, M. Kitano, H. J. Chiang, L. A. Trinh, G. Turcatel, B. Steventon, C. Arnesano, D. Warburton, S. E. Fraser, and F. Cutrale, "Pre-processing visualization of hyperspectral fluorescent data with Spectrally Encoded Enhanced Representations," Nature Communications 11(1), 726 (2020).

35. Z. Zhou, M. M. Rahman Siddiquee, N. Tajbakhsh, and J. Liang, "UNet++: A Nested U-Net Architecture for Medical Image Segmentation," in Deep Learning in Medical Image Analysis and Multimodal Learning for Clinical Decision Support, D. Stoyanov, Z. Taylor, G. Carneiro, T. Syeda-Mahmood, A. Martel, L. Maier-Hein, J. M. R. S. Tavares, A. Bradley, J. P. Papa, V. Belagiannis, J. C. Nascimento, Z. Lu, S. Conjeti, M. Moradi, H. Greenspan, and A. Madabhushi (Eds.), Springer International Publishing, 11045, 3–11 (2018).
36. W. Tingxi, T. Binbin, L. Yu, P. Ting, D. Yu, C. Yuping, and Z. Shanshan, "Review of research on the instance segmentation of cell images," Computer Methods and Programs in Biomedicine 227, 107211 (2022).
37. S. M. A. Burney, H. Tariq, "K-Means Cluster Analysis for Image Segmentation," International Journal of Computer Applications 96(4), 1–8 (2014).
38. W. Gao, "Random Forest in Image Segmentation," Machine Learning Theory and Practice 1, 11–19 (2020).
39. Z. Kato, "Markov Random Fields in Image Segmentation," Foundations and Trends® in Signal Processing 5(1–2), 1–155 (2011).
40. B. Karthicsonia, M. Vanitha, "Edge Based Segmentation in Medical Images," International Journal of Engineering and Advanced Technology 9(1), 449–451 (2019).
41. O. Ronneberger, P. Fischer, and T. Brox, "U-Net: Convolutional Networks for Biomedical Image Segmentation," in Medical Image Computing and Computer-Assisted Intervention – MICCAI 2015, N. Navab, J. Hornegger, W. M. Wells, and A. F. Frangi (Eds.), Springer International Publishing, 9351, 234–241 (2015).
42. D. Bannon, E. Moen, M. Schwartz, E. Borba, T. Kudo, N. Greenwald, V. Vijayakumar, B. Chang, E. Pao, E. Osterman, W. Graf, and D. Van Valen, "DeepCell Kiosk: scaling deep learning–enabled cellular image analysis with Kubernetes," Nature Methods18(1), 43–45 (2021).
43. A. E. Carpenter, T. R. Jones, M. R. Lamprecht, C. Clarke, I. H. Kang, O. Friman, D. A. Guertin, J. H. Chang, R. A. Lindquist, J. Moffat, P. Golland, and D. M. Sabatini, "CellProfiler: image analysis software for identifying and quantifying cell phenotypes," Genome Biology 7(10), R100 (2006).
44. K. He, X. Zhang, S. Ren, and J. Sun, "Spatial Pyramid Pooling in Deep Convolutional Networks for Visual Recognition," IEEE Transactions on Pattern Analysis and Machine Intelligence 37(9), 1904–1916 (2015).
45. Y. Wang, W. Wang, D. Liu, W. Hou, T. Zhou, and Z. Ji, "GeneSegNet: a deep learning framework for cell segmentation by integrating gene expression and imaging," Genome Biology 24(1), 235 (2023).
46. J. Wu, R. Fu, H. Fang, Y. Zhang, Y. Yang, H. Xiong, H. Liu, and Y. Xu, "MedSegDiff: Medical Image Segmentation with Diffusion Probabilistic Model," in Medical Imaging with Deep Learning, Proceedings of Machine Learning Research 227, 1623–1639 (2024).
47. J. Ma, F. Li, and B. Wang, "U-Mamba: Enhancing Long-range Dependency for Biomedical Image Segmentation," arXiv preprint arXiv:2401.04722 (2024).
48. J. Ruan, S. Xiang, "VM-UNet: Vision Mamba UNet for Medical Image Segmentation," arXiv preprint arXiv:2402.02491 (2024).
49. Z. Xing, T. Ye, Y. Yang, G. Liu, and L. Zhu, "SegMamba: Long-range Sequential Modeling Mamba For 3D Medical Image Seg-mentation," in International Conference on Medical Image Computing and Computer-Assisted Intervention, Springer Nature Switzerland, Cham, 578–588 (2024).
50. Z. Lu, C. She, W. Wang, and Q. Huang, "LM-Net: A light-weight and multi-scale network for medical image segmentation," Computers in Biology and Medicine 168, 107717 (2024).
51. C. You, W. Dai, Y. Min, F. Liu, D. Clifton, S. K. Zhou, L. Staib, and J. Duncan, "Rethinking Semi-Supervised Medical Image Segmentation: A Variance-Reduction Perspective," Advances in neural information processing systems, 36, 9984–10021 (2023).
52. D. Müller, I. Soto-Rey, and F. Kramer, "Towards a guideline for evaluation metrics in medical image segmentation," BMC Research Notes 15(1), 210 (2022).
53. H. Khastavaneh, H. Ebrahimpour-komleh, "Automated Segmentation of Abnormal Tissues in Medical Images," Journal of Biomedical Physics & Engineering 11(4), 415–424 (2019).
54. P. Qin, J. Chen, J. Zeng, R. Chai, and L. Wang, "Large-scale tissue histopathology image segmentation based on feature pyramid," EURASIP Journal on Image and Video Processing 2018, 75 (2018).
55. A. K. Kuchibhotla, L. D. Brown, A. Buja, and J. Cai, "All of Linear Regression," arXiv preprint arXiv:1910.06386 (2019).
56. H.-H. Huang, Q. He, "Nonlinear regression analysis," in International Encyclopedia of Education, 4th Ed., Elsevier, 558–567 (2023).
57. R. S. Turley, "Polynomial Fitting", Faculty Publication, 2237, 1 Jan 2018 (accessed 22 October 2024). [https://scholarsarchive.byu.edu/facpub/2237].
58. D. C. Vargas, E. J. Rodríguez, M. Flickner, and J. L. C. Sanz, "Splines and Spline Fitting Revisited," in Image Technology: Advances in Image Processing, Multimedia and Machine Vision, J. L. C. Sanz (Ed.), Springer Berlin Heidelberg, 405–437 (1996).
59. M. Li, L. D. Li, "A Novel Method of Curve Fitting Based on Optimized Extreme Learning Machine," Applied Artificial Intelligence 34(12), 849–865 (2020).

60. V. P, D. R. Rao, "Machine Learning Techniques on Multidimensional Curve Fitting Data Based on R- Square and Chi-Square Methods," International Journal of Electrical and Computer Engineering 6(3), 974–979 (2016).
61. S. S. Sidharth, "Curve Fitting Simplified: Exploring the Intuitive Features of CurvPy," arXiv preprint arXiv:2307.06377 (2023).
62. N. Tumbarkova, N. Deliiski, "Applying the software package TableCurve 2D for computation of processing air medium temperature during freezing in a freezer and defrosting of logs," Innovations in Woodworking Industry and Engeneering Design 11, 69–76 (2017).
63. A. Dakkak, T. Wickham-Jones, and W.-m. Hwu, "The design and implementation of the wolfram language compiler," Proceedings of the 18th ACM/IEEE International Symposium on Code Generation and Optimization, San Diego, CA, USA, 212–228 (2020).
64. T. Cepowski, ndCurveMaster (8.7), SigmaLab [Computer Software], (2025) (accessed 22 October 2024). [https://www.ndcurvemaster.com].
65. D. Gao, P. R. Barber, J. V. Chacko, Md. A. Kader Sagar, C. T. Rueden, A. R. Grislis, M. C. Hiner, and K. W. Eliceiri, "FLIMJ: An open-source ImageJ toolkit for fluorescence lifetime image data analysis," PLoS ONE 15(12), e0238327 (2020).
66. D. Nečas, P. Klapetek, "Gwyddion: an open-source software for SPM data analysis," Central European Journal of Physics 10, 181–188 (2011).
67. L. Hu, N. Wang, J. D. Bryant, L. Liu, L. Xie, A. P. West, and A. J. Walsh, "Machine learning prediction of cancer cell metabolism from autofluorescence lifetime images," bioRxiv [preprint], 2022.2012.16.520759 (2022).
68. N. I. Nizam, V. Pandey, I. Erbas, J. T. Smith, and X. Intes, "A Novel Technique for Fluorescence Lifetime Tomography," bioRxiv [preprint], 2024.09.19.613888 (2024).
69. D. Xiao, N. Sapermsap, Y. Chen, and D. D. U. Li, "Deep learning enhanced fast fluorescence lifetime imaging with a few photons," Optica 10(7), 944 (2023).
70. Z. Zang, D. Xiao, Q. Wang, Z. Jiao, Y. Chen, and D. D. U. Li, "Compact and robust deep learning architecture for fluorescence lifetime imaging and FPGA implementation," Methods and Applications in Fluorescence 11(2), 025002 (2023).
71. D. Xiao, Y. Chen, and D. D.-U. Li, "One-Dimensional Deep Learning Architecture for Fast Fluorescence Lifetime Imaging," IEEE Journal of Selected Topics in Quantum Electronics 27(4), 1–10 (2021).
72. Q. Wang, Y. Li, D. Xiao, Z. Zang, Z. Jiao, Y. Chen, and D. D. U. Li, "Simple and Robust Deep Learning Approach for Fast Fluorescence Lifetime Imaging," Sensors 22(19), 7293 (2022).
73. Y.-I. Chen, Y.-J. Chang, S.-C. Liao, T. D. Nguyen, J. Yang, Y.-A. Kuo, S. Hong, Y.-L. Liu, H. G. Rylander, S. R. Santacruz, T. E. Yankeelov, and H.-C. Yeh, "Deep learning enables rapid and robust analysis of fluorescence lifetime imaging in photon-starved conditions," bioRxiv [preprint], 2020.2012.02.408195 (2020).
74. F. Wang, S. H. Kim, Y. Zhao, A. Raghuram, A. Veeraraghavan, J. Robinson, and A. H. Hielscher, "High-Speed Time-Domain Diffuse Optical Tomography With a Sensitivity Equation-Based Neural Network," IEEE Transactions on Computational Imaging 9, 459–474 (2023).
75. M. Fazel, S. Jazani, L. Scipioni, A. Vallmitjana, S. Zhu, E. Gratton, M. A. Digman, and S. Pressé, "Building Fluorescence Lifetime Maps Photon-by-Photon by Leveraging Spatial Correlations," ACS Photonics 10(10), 3558–3569 (2023).
76. D.-M. Koh, N. Papanikolaou, U. Bick, R. Illing, C. E. Kahn, J. Kalpathi-Cramer, C. Matos, L. Martí-Bonmatí, A. Miles, S. K. Mun, S. Napel, A. Rockall, E. Sala, N. Strickland, and F. Prior, "Artificial intelligence and machine learning in cancer imaging," Communications Medicine 2(1), 133 (2022).
77. V. Mannam, Y. Zhang, X. Yuan, C. Ravasio, and S. S. Howard, "Machine learning for faster and smarter fluorescence lifetime imaging microscopy," Journal of Physics: Photonics 2(4), 042005 (2020).
78. N. Thuerey, P. Holl, M. Mueller, P. Schnell, F. Trost, and K. Um, "Physics-based Deep Learning," arXiv preprint arXiv:2109.05237 (2021).
79. A. Arzani, L. Yuan, P. Newell, and B. Wang, "Interpreting and generalizing deep learning in physics-based problems with functional linear models," Engineering with Computers 41(1), 135–157 (2025).
80. Y. Sun, Q. Sun, and K. Qin, "Physics-Based Deep Learning for Flow Problems," Energies 14(22), 7760 (2021).
81. D. Zhang, Y. Chen, and S. Chen, "Filtered partial differential equations: a robust surrogate constraint in physics-informed deep learning framework," Journal of Fluid Mechanics 999, A40 (2024).
82. S. Kaltenbach, P.-S. Koutsourelakis, "Incorporating physical constraints in a deep probabilistic machine learning framework for coarse-graining dynamical systems," Journal of Computational Physics 419, 109673 (2020).